# Boron transport simulation using the ERO2.0 code for real-time wall conditioning in the Large Helical Device

**M. Shoji**<sup>a</sup>, G. Kawamura<sup>a,b</sup>, J. Romazanov<sup>c</sup>, A. Kirschner<sup>c</sup>, A. Eksaeva<sup>c</sup>, D. Borodin<sup>c</sup>, S. Masuzaki<sup>a,b</sup>, S. Brezinsek<sup>c</sup>

<sup>a</sup>National Institute for Fusion Science, National Institutes of Natural Sciences, 322-6 Oroshi-cho, Toki 509-5292, Japan

<sup>b</sup>The Graduate University for Advanced Studies (SOKENDAI), Shonan Village, Hayama 240-0913, Japan <sup>c</sup>Forschungszentrum Jülich GmbH, Institut für Energie- und Klimaforschung - Plasmaphysik, Partner of the Trilateral Euregio Cluster (TEC), Jülich 52425, Germany

shoji@nifs.ac.jp

#### **Abstract**

A three-dimensional Monte-Carlo impurity transport and plasma-surface interaction code ERO2.0 is applied to a full-torus model for the Large Helical Device (LHD). In order to find an optimum experimental condition for effective real-time wall conditioning (boronization) using an Impurity Powder Dropper (IPD), the toroidal and poloidal profile of the boron deposition density on the divertor components and the vacuum vessel are surveyed in various experimental conditions. The three-dimensional distribution of the atomic boron source in the peripheral plasma originated from boron powders supplied from the IPD is calculated using the DUSTT in background plasmas provided by the EMC3-EIRENE. The simulations using the ERO2.0 prove that higher plasma density operation is inappropriate for the wall conditioning because of localized boron deposition in a closed helical divertor region. The ERO2.0 have successfully revealed an optimum experimental condition for effective wall conditioning with toroidally uniform boron deposition in the closed divertor region.

Keywords: ERO2.0, impurity powder dropper, DUSTT, EMC3-EIRENE, LHD, boronization

#### 1. Introduction

It is well known that wall conditioning is quite effective for high-performance plasma discharges by reducing the impurity radiation in the peripheral plasma, and the control of neutral particle recycling in the divertor region [1]. In the Large Helical Device (LHD), helium glow discharge cleaning (GDC) with diborane gas has been routinely applied as a conventional wall conditioning (boronization) method for about these two decades [2]. One of the fatal disadvantage of this conventional method is the difficulty of boron deposition in the closed helical divertor (CHD) region in the inboard side of the torus. This is because the CHD is located in a narrow recessed area from the GDC plasma and the divertor plates in the CHD region do not face to the GDC plasma.

In order to overcome this disadvantage, a wall conditioning method which is so called "the real-time boronization" was proposed [3]. An impurity powder dropper (IPD), which has been developed in the Princeton Plasma Physics Laboratory, was installed in one of the upper ports in the last experimental campaign in the fiscal year 2019 [4]. The boronization using the IPD was firstly tried and contributed to the reduction of the impurity radiation to a certain extent [5]. The boron atoms contained in boron powders supplied from the IPD are evaporated and ionized in the peripheral plasma. The resultant boron ions are transported to the divertor

region along the magnetic field lines in the peripheral plasma, which contributes to the deposition of boron in the divertor region and leads to an effective wall conditioning in LHD.

With a view to making the full use of the potential of the IPD, an experimental condition which is appropriate for the effective wall conditioning has to be found in advance before this device will be routinely used hereafter. For this purpose, a three-dimensional Monte-Carlo impurity transport and plasma-surface interaction code ERO2.0 was firstly applied to LHD [6]. The toroidal and poloidal profile of the boron density deposited on the surfaces of the divertor components and the vacuum vessel is calculated in various experimental conditions using a three-dimensional full-torus model specialized for the ERO2.0. It is expected that the simulations provide a useful guideline for realizing high-performance plasma discharges using the IPD in future experimental campaigns.

# 2. Set up for the simulation of boron transport and deposition using the ERO2.0 in the Large Helical Device

The LHD is one of the world's largest heliotron type machines having super-conducting helical coils and poloidal coils to produce magnetic field line configurations for confining helically twisted shaped plasma without the toroidal plasma current. The major and averaged plasma minor radii of the typical plasma are about 3.6 m and 0.6 m, respectively [7]. An ergodized magnetic field line structure are intrinsically formed in the peripheral plasma outside of the Last Closed Flux Surface (LCFS), which is called as an ergodic layer, and four bundled magnetic field lines (divertor legs) are formed in the divertor region. The magnetic field lines in the peripheral plasma are directly connected to the vacuum vessel (stainless steel) and divertor plates made of isotropic graphite (carbon).

The impurity transport and plasma-surface interaction simulation using ERO2.0 are performed in fixed background (BG) deuterium plasmas provided by the fully three-dimensional edge plasma simulation code (EMC3-EIRENE) [8, 9]. The BG plasma parameter profiles in a full-torus grid model ( $0^{\circ} \le \phi \le 360^{\circ}$  in toroidal direction  $\phi$ ) are created by toroidally extending the simulation results in one-half of the helical coil pitch angle  $(0^{\circ} \le \phi \le 18^{\circ})$ with the assumption of up-and-down and toroidally periodic symmetry. The profiles are obtained from the calculations in an inward-shifted magnetic configuration in which the radial position of the magnetic axis  $R_{\rm ax}$  equals to 3.60 m and the toroidal magnetic field direction is counter-clockwise. The EMC3-EIRENE calculates the BG plasma parameter profiles under a boundary condition where the plasma heating power and the plasma density at an inner boundary locating just inside of the LCFS ( $P^{LCFS}$  and  $n_e^{LCFS}$  respectively) are fixed to constant values. The perpendicular particle and the ion/electron thermal diffusion coefficients are assumed to be 0.5 and 1.0 m<sup>2</sup>/s, respectively, which is typical values for explaining the measured plasma density and temperature profiles in the peripheral plasma. It is assumed that the divertor components (closed helical divertor plates, dome plates, and open divertor plates) and the vacuum vessel in the full-torus model have a 10 cycled toroidal periodicity. An open divertor structure in one helical section in the actual LHD configuration is not included in this full-torus model. The divertor components and the vacuum vessel in this model consist of the groups of small triangle surfaces being less than a few cm in length. The materials consisting of the divertor components and the vacuum vessel are treated as carbon and iron, respectively.

The three-dimensional distribution of an impurity source (neutral boron atoms) in the peripheral plasma has to be defined for the ERO2.0 as an initial input parameter for the impurity transport simulation. The distribution of the neutral boron atoms originating from the

boron powders supplied from the IPD is derived from the simulation results using a dust transport simulation code (DUSTT) [10-12]. In the DUSTT, a spherical pure boron powder is injected downward with a velocity of 5.0 m/s from an initial position locating in a grid model for the one-half of the helical coil pitch angle  $(0^{\circ} \le \phi \le 18^{\circ})$  which is specially prepared for calculating the three-dimensional trajectory of boron powders dropped from the IPD installation position. The downward velocity approximately corresponds to the falling speed at the initial position on the free fall trajectory. Because the IPD is installed in an upper port in a helical section with the open divertor structure, the CHD components are not included in this grid model. The DUSTT calculates the three-dimensional trajectory of the boron powders by solving the equation of the time evolution of the motion, heat, energy, size and charge balances in a fixed BG plasma parameter profiles (the plasma density and the ion/electron temperature, the plasma flow velocity and so on) provided by the EMC3-EIRENE. When the boron powders reach the peripheral plasma, the temperature of the powder rises by the plasma heat load, and the temperature finally reaches the boiling point. The distribution of the neutral atomic boron source is defined as the boron evaporation rate at the positions along the trajectory of the powder.

Figure 1 illustrates a perspective view of the three-dimensional grid model for calculating the boron powder trajectories dropped from the IPD. The initial position for tracing the powders is indicated as a small yellow circle locating close to an upper divertor leg. An outlet for dropping the powders is actually installed above ~2 m from the initial position. The gravity acts on toward –Z direction (downward) in this figure. A poloidal cross-section of grids representing the LHD peripheral plasma (the ergodic layer and the divertor legs) is shown, which is the cross-section at a toroidal angle  $\phi$  of -6.125° at which the IPD is installed (the LHD plasma is vertically elongated at  $\phi = 0$ °).

The three-dimensional distribution of the neutral atomic boron source is one of the essential parameters for investigating the performance of the wall-conditioning using the IPD. Thus, the boron powder trajectory in the peripheral plasma in various experimental conditions are surveyed by changing the plasma density  $n_e^{\text{LCFS}}$ , the boron powder size (diameter)  $d_B$ , and the plasma heating power  $P^{LCFS}$ . Figure 2 (a) gives the trajectories for two different BG plasma densities ( $n_e^{\text{LCFS}} = 1 \times 10^{19} \text{ m}^{-3}$  and  $4 \times 10^{19} \text{ m}^{-3}$  with  $P^{\text{LCFS}} = 8 \text{ MW}$ ) for a powder diameter  $d_B$  of 150 µm. The position of the area displayed in Figure 2 is shown as a red broken square in Figure 1. The points where the boron powders are completely evaporated are indicated as coloured open circles as a simple indicator for representing the penetration of the powders into the plasma. It should be noted that the atomic boron sources are distributed along the powder trajectory to the point of the open circles (evaporation position). The trajectories show that the boron powders have to pass through the upper divertor leg before reaching the ergodic layer. For the higher plasma density ( $n_e^{\text{LCFS}}=4\times10^{19} \text{ m}^{-3}$ ), the trajectory of the boron powder is considerably deflected at the divertor leg due to the effect of the plasma flow (the ion drag force directed to the divertor plates), which results in the evaporation position at the edge of the ergodic layer, which is indicated as a grey open circle in Figure 1 (a). Compared to the high plasma density case, the evaporation position for the low plasma density ( $n_e^{\text{LCFS}}=1\times10^{19} \text{ m}^{-3}$ ) locates in the deeper region in the ergodic layer, which is due to the smaller deflection of the trajectory because of the lower ion drag force in the divertor leg.

The calculated boron powder trajectories for various powder sizes  $d_{\rm B}$  are presented in Figure 2 (b), in which the plasma density  $n_{\rm e}^{\rm LCFS}$  and the heating power  $P^{\rm LCFS}$  are set to be  $1\times10^{19}$  m<sup>-3</sup> and 8 MW, respectively. The powder sizes are changed from 100  $\mu$ m to 200  $\mu$ m in

diameter (the nominal maximum tolerable diameter is 200 µm for the IPD). Larger powders tend to penetrate into the deeper region in the ergodic layer. The larger the powder size is, the more the evaporated position relatively approaches the core plasma, which is due to the fact that the increment of the powder temperature becomes smaller due to the larger heat capacity. The deflection of the trajectories of the larger sized powders at the divertor leg is more moderate, which is due to the inertia of the heavier (larger) powders. These two contribute to moving the evaporation position of the boron powders to a higher plasma temperature region close to the core plasma.

Figure 2 (c) presents boron powder trajectories for four different plasma heating powers  $P^{\rm LCFS}$  under the condition where the plasm density  $n_{\rm e}^{\rm LCFS}$  is  $1\times10^{19}$  m<sup>-3</sup> and the powder size  $d_{\rm B}$  is 150 µm. The evaporation positions of the boron powders are drastically changed with the plasma heating power. The lower the plasma heating power is, the more the evaporated position approaches the core plasma because of the lower plasma heat load on the powders which make the powders penetrate into the deeper region in the peripheral plasma.

The neutral boron atoms released from the evaporated boron powders are traced by the ERO2.0 in the full-torus model. The boron atoms are assumed to be immediately ionized in the plasma. A large number (in the order of one million) of test particles (representative evaporated boron atoms) are launched from the birth points of the boron atoms. The weighting ratio of the number of the test particles is in proportion to the boron evaporation rate calculated by the DUSTT at the birth points. In this simulation, the dropping rate of the numbers of the boron atoms contained in the powders is assumed to be  $6.24 \times 10^{15}$  atoms/s which is found to be negligibly small for perturbing the BG plasmas [13]. The ERO2.0 tracks boron ion trajectories in the peripheral plasma with a diffusion coefficient of 1.0 m²/s and the ionization/recombination rates derived from the database on the Atomic Data and Analysis Structure (ADAS) [14].

The boron atoms/ions colliding with the vacuum vessel and the divertor components are deposited or reflected on the surfaces. The boron atoms/ions induce the sputtering on the vacuum vessel and the divertor components. The angular and the energy dependences of the reflection coefficients/the sputtering yields are provided by simulations using the SDTrimSP for specified projectile-target combinations (boron on carbon and boron on iron) [15]. The erosion of the deposited boron by the plasma (deuterium ion), sputtered carbon, and sputtered iron atoms is not included. The boron self-sputtering is also not included, meaning that the simulation corresponds to a so-called "the first time step calculation" in the ERO2.0.

# 3. Full-torus boron transport simulation for finding an optimum plasma discharge condition for effective wall conditioning

In order to find an optimum experimental condition for the wall conditioning using the IPD, full-torus boron transport simulation was performed using the ERO2.0 in various experimental conditions. Figure 3 is a perspective view of a simulation result of the full-torus distribution of the boron areal density deposited on the surfaces of the divertor components (the vacuum vessel is not shown). In this simulation, the boron powder size  $d_B$  is 150  $\mu$ m, the plasma density  $n_e^{LCFS}$  is  $4\times10^{19}$  m<sup>-3</sup>, and the plasma heating power  $P^{LCFS}$  is set to be 8 MW. The colour on the divertor components indicate the areal density of the deposited boron atoms. It should be noted that the back plates of the divertor components are not displayed in this figure, which means that the boron density deposited on the front surfaces of the divertor components is seen from the backside. This figure shows that while the boron is distributed along the strike

points (the plasma wetted areas) on the divertor plates, the toroidal distribution of the boron density is not uniform. That is, the boron density on the closed helical divertor plates in the inboard side installed in a helical section adjacent to the IPD installation position is considerably higher than that in the other helical sections. This extremely localized boron deposition is unfavourable for the effective wall conditioning for reducing overall impurities in LHD plasmas.

For finding an experimental condition for toroidally uniform boron deposition especially in the CHD region, the following three parameters are surveyed in the simulation: the plasma density  $n_e^{\text{LCFS}}$ , the boron powder size (diameter)  $d_B$ , and the plasma heating power  $P^{\rm LCFS}$ . With a view to entirely displaying the boron deposition density in the torus, the boron areal density is displayed on the full-torus toroidal and poloidal plane as a two-dimensional grey-scale plot. Figure 4 (a) and (b) show the simulations of the boron areal density profile for low and high plasma densities ( $n_e^{\text{LCFS}}=1\times10^{19} \text{ m}^{-3}$  and  $4\times10^{19} \text{ m}^{-3}$  with  $P^{\text{LCFS}}=8 \text{ MW}$  and  $d_{\rm B}$ =150 µm), respectively. The boron density deposited on the dome plates is not included in the figures. A small yellow circle approximately shows the initial position for tracing the boron powder trajectories projected onto the toroidal and poloidal plane. The two figures indicate that, in the high plasma density case, the deposition density is significantly localized (a) compared to that in the low plasma density case (b). For the high plasma density, the boron deposition density is extremely high in the CHD region where the poloidal angle  $\theta$  is in the range 120°≤θ≤240° with a toroidal angle of around 342°. This position corresponds to the helical section where the boron deposition density is extremely high in the CHD region as shown in Figure 3. This highly localization is due to the high boron ion flux density from the evaporation position of the boron powders in the peripheral plasma in an adjacent helical section. As shown in Figure 2 (a), the boron powders generate an atomic boron source in the outer edge of the ergodic layer where the connection length of the magnetic field lines  $L_{\mathbb{C}}$  is very short (in the order of several meters) [16]. For the high plasma density, most of the resultant boron ions are transported to the adjacent CHD region along the magnetic field lines. In addition to this, the CHD region is surrounded by the divertor components such as the inclined divertor plates and the dome plates in the narrow space, which enhances the deposition of the reflected and sputtered boron atoms in this region [17]. Additionally, the ERO2.0 simulation clarifies that the boron deposition density is quite high on the surface of a helical coil can in the inboard side (the poloidal angle  $\theta$ -180°) at a toroidal angle of around 324° (close to the above CHD region). This is because the helical coil can is extruded from the surface of the vacuum vessel toward the LHD plasma, leading to the boron deposition on the helical coil can. The simulation results using the ERO2.0 reveals that the high plasma density is inappropriate for the effective wall-conditioning with the toroidally uniform boron deposition.

It is expected that the increase in the boron powder size can contribute to more toroidally uniform boron deposition because larger boron powders are fully evaporated in the deeper region in the peripheral plasma where the connection length  $L_{\rm C}$  is longer by which the resultant boron ions can be transported to the divertor region locating far from the IPD installation position [16]. Figure 5 (a) and (b) display the boron deposition density profile for two powder sizes ( $d_{\rm B}$ =100 µm and 200 µm) under the low plasma density  $n_{\rm e}^{\rm LCFS}$ =1×10<sup>19</sup> m<sup>-3</sup> with  $P^{\rm LCFS}$ =8 MW, respectively. In the both cases, the calculated boron deposition density on the helical coil can in the inboard side of the torus is relatively high at toroidal angles of 180° and 324°. The boron deposition density in the CHD region next to these two toroidal angles ( $\theta$ ~162° and 342°) is also higher than that at the other toroidal angles. The simulations suggest

that the increase in the powder size is not so effective for improving the toroidal uniformity of the boron deposition in the divertor region. One of the reason for the no significant difference of the deposition density profiles in both powder sizes is attributed to the roughly equivalent distribution of the neutral atomic boron sources along the trajectories in the ergodic layer where the  $L_{\rm C}$  is relatively short in the both cases. The ERO2.0 demonstrates that the increase in the powder size in the range between 100  $\mu$ m and 200  $\mu$ m is not appropriate for enhancing the wall conditioning.

The change of the plasma heating power drastically affects the evaporation position of the boron powders as shown in Figure 2 (c). Lower plasma heating powers are expected to be appropriate for more toroidally uniform boron deposition in the divertor region because the evaporated position in lower heating powers is close to the core plasma where the connection length  $L_C$  is very long (more than 10 kilometers). Figure 6 (a) and (b) give the simulations of the boron deposition density profile for two low plasma heating powers ( $P^{\text{LCFS}}=2$  MW and 1 MW) under the condition of the low plasma density  $n_e^{\text{LCFS}}=1\times10^{19}$  m<sup>-3</sup> with  $d_B=150$  µm, respectively. Compared to the profile for the high plasma heating power ( $P^{\text{LCFS}}=8$  MW) as shown in Figure 4 (a), the toroidal uniformity of the boron density in the divertor region and on the helical coil can is significantly improved, where the boron deposition density on the helical coil can at the two toroidal angles (180° and 324°) is not considerably higher than that at the other helical coil cans. The ERO2.0 simulations prove that the lower plasma heating power operation ( $P^{\text{LCFS}}\leq 2$  MW) is quite effective for improving the toroidal uniformity of the boron deposition in the divertor region and on the helical coil cans, which is favourable for the effective wall conditioning using the IPD as far as the plasma is not terminated by the radiation collapse [18].

### 4. Summary

In order to find an optimum experimental condition for effective wall conditioning (boronization) using the IPD, full-torus boron transport simulation was performed using the ERO2.0 under background plasmas calculated by the EMC3-EIRENE coupled with neutral atomic boron source distributions provided by the DUSTT. The full-torus toroidal and poloidal profile of the deposited boron density is calculated in various experimental conditions by changing the following three parameters: the plasma density  $n_e^{\text{LCFS}}$ , the boron powder size (diameter)  $d_{\rm B}$ , and the plasma heating power  $P^{\rm LCFS}$ . The simulations show that the higher plasma density ( $n_e^{\text{LCFS}}=4\times10^{19} \text{ m}^{-3}$ ) is undesirable for achieving toroidally uniform boron deposition in the divertor region and on the helical coil can. This is because the boron evaporation position locates in the outer edge of the ergodic layer, which is caused by the deflection of the trajectory of the boron powder due to the plasma flow in the upper divertor leg. The simulation also indicates that the increase in the powder size is not so effective for improving the toroidal uniformity of the boron deposition. The ERO2.0 proves that the lower plasma heating power ( $P^{LCFS} \le 2$  MW) with the low plasma density ( $n_e^{LCFS} = 1 \times 10^{19}$  m<sup>-3</sup>) is quite effective for the toroidally uniform boron deposition, which can contribute to the effective wall conditioning using the IPD for high-performance plasma discharges in LHD.

### Acknowledgments

This work is performed under the auspices of the NIFS Collaboration Research program (NIFS12KNXN236). The author would like to thank Y. Feng for permission to use the EMC3-EIRENE. He is also grateful to Profs. S. I. Krasheninnikov and Y. Tanaka, and Dr. R. D. Smirnov for providing the DUSTT, and for the support for using the code in our computational

environment. Furthermore, he appreciates the computational resources of the LHD numerical analysis server and the plasma simulator in NIFS. This work is also supported by JSPS KAKENHI Grant Numbers 18H01203, 16H04619, and 16K18340.

- [1] J. Winger et al., Plasma Phys. Control. Fusion **38** (1996) 1503.
- [2] K. Nishimura et al., J. Nucl. Mater. 337 (2005) 431.
- [3] A. Sagara et al., J. Nucl. Mater. **241-243** (1997) 972.
- [4] A. Nagy et al., Rev. Sci. Instrum. **89** (2018) 10K121.
- [5] N. Federico et al., These proceedings for PSI2020.
- [6] J. Romazanov et al., Nucl. Mater. Energy 18 (2019) 331.
- [7] Y. Takeiri et al., Nucl. Fusion **57** (2017) 102023.
- [8] Y. Feng et al., Plasma Phys. Control. Fusion 44 (2002) 611.
- [9] G. Kawamura et al., Contrib. Plasma Phys. **54** (2014) 437.
- [10] A. Yu Pigarov et al., J. Nucl. Mater. **363-365** (2007) 216.
- [11] R. D. Smirnov et al., Plasma Phys. Control Fusion 49 (2007) 347.
- [12] Y. Tanaka et al., J. Nucl. Mater. 415 (2011) S1106.
- [13] M. Shoji et al., Contrib. Plasma Phys. (to be published).
- [14] The ADAS User Manual (version 2.6) http://adas.phys.strath.ac.uk/ (2004).
- [15] W. Möller et al., Comput. Phys. Commun. 51 (1988) 355.
- [16] T. Watanabe et al., Nucl. Fusion 46 (2006) 291.
- [17] M. Shoji et al., Contrib. Plasma Phys. **56** (2016) 651.
- [18] B. J. Peterson et al., Phys. Plasmas. 8 (2001) 3861.

## **Figures**

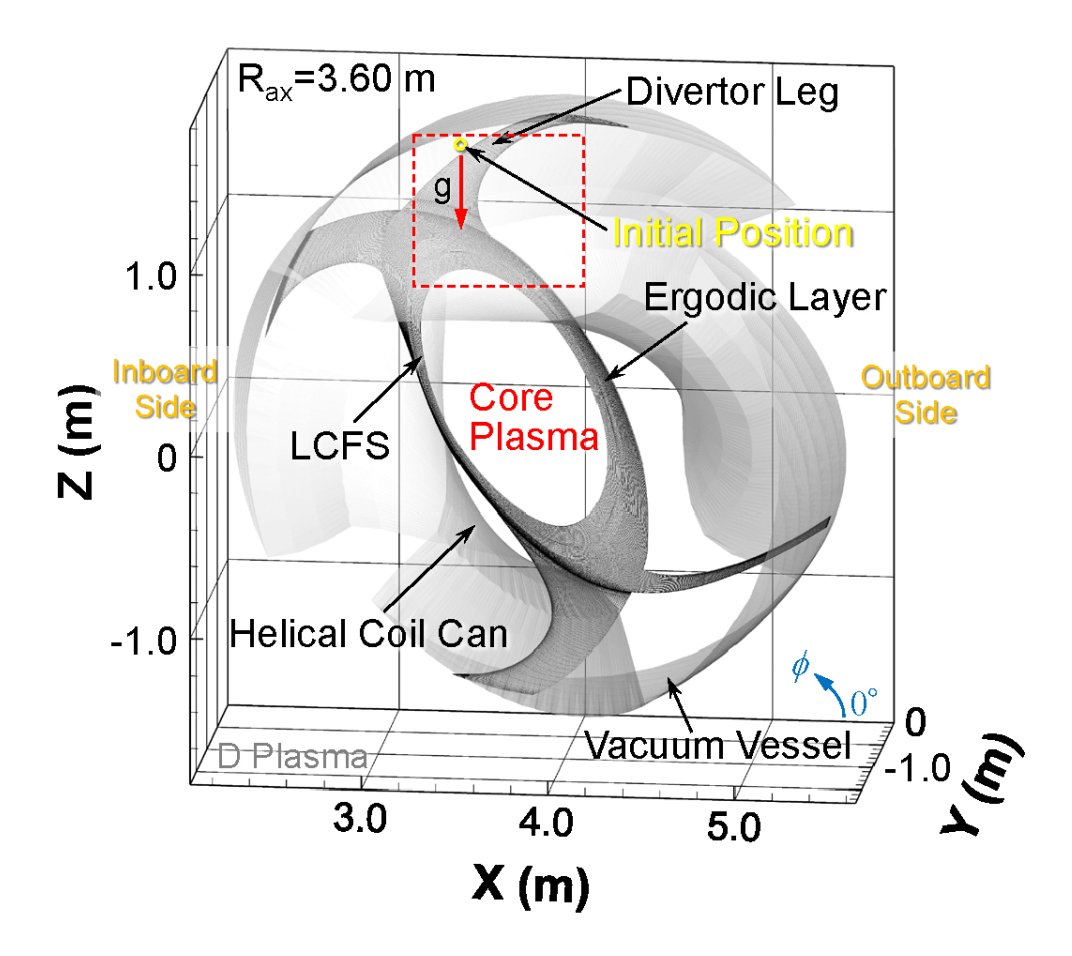


Fig. 1. A perspective view of a three-dimensional grid model for the one-half of the helical coil pitch angle  $(0^{\circ} \le \phi \le 18^{\circ})$  for calculating the trajectory of boron powders dropped from the IPD. An open yellow circle indicates the initial position for tracing the trajectories. This model includes the geometrical structure of the vacuum vessel and the LHD peripheral plasma (the ergodic layer and the divertor legs). The poloidal cross-section of the grids for the peripheral plasma at the toroidal angle, at which the IPD is installed, is presented in this figure.

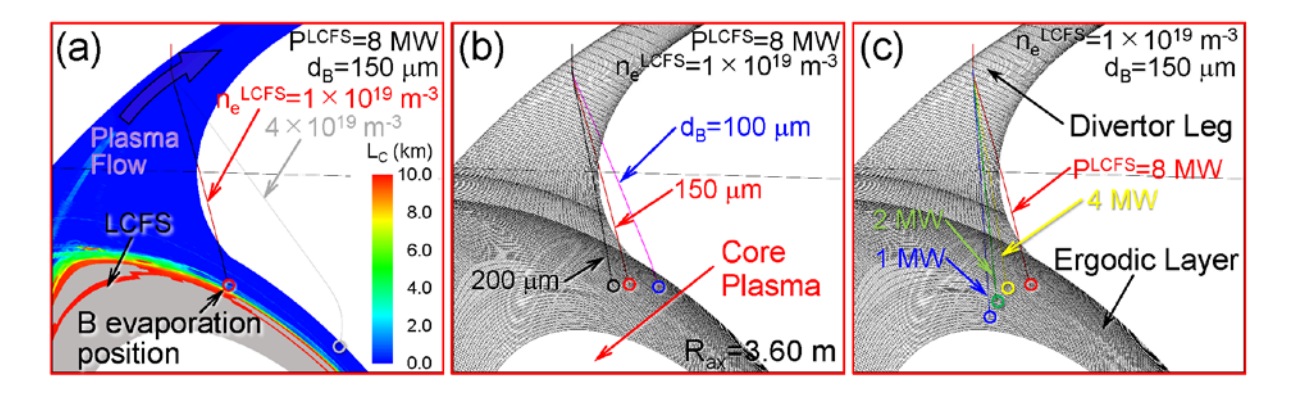


Fig. 2.

(a) The calculations of the dropped boron powder trajectories in the case of the low and high plasma densities ( $n_e^{\text{LCFS}} = 1 \times 10^{19} \text{ m}^{-3}$  and  $4 \times 10^{19} \text{ m}^{-3}$ , respectively) for the plasma heating power  $P^{\text{LCFS}} = 8$  MW and the boron powder size (diameter)  $d_B = 150 \, \mu \text{m}$ . The poloidal cross-section of the connection length of the magnetic field lines  $L_C$  in the peripheral plasma is presented (the grey area inside around the LCFS indicates the region where the connection length is more than 10 km). (b) The calculated boron powder trajectories for three different powder sizes  $d_B$  in the range from 100  $\mu$ m to 200  $\mu$ m for  $P^{\text{LCFS}} = 8$  MW and  $n_e^{\text{LCFS}} = 1 \times 10^{19} \, \text{m}^{-3}$ . The poloidal cross-section of the grid meshes for the LHD peripheral plasma is illustrated. (c) The trajectories of the boron powder for four different plasma heating powers  $P^{\text{LCFS}}$  in the range from 1 MW to 8 MW in the case of  $n_e^{\text{LCFS}} = 1 \times 10^{19} \, \text{m}^{-3}$  and  $d_B = 150 \, \mu \text{m}$ . The positions where the boron powders are completely evaporated by the plasma heat load are indicated as coloured small open circles. The position of the area displayed in this figure is indicated as a red broken square in Figure 1.

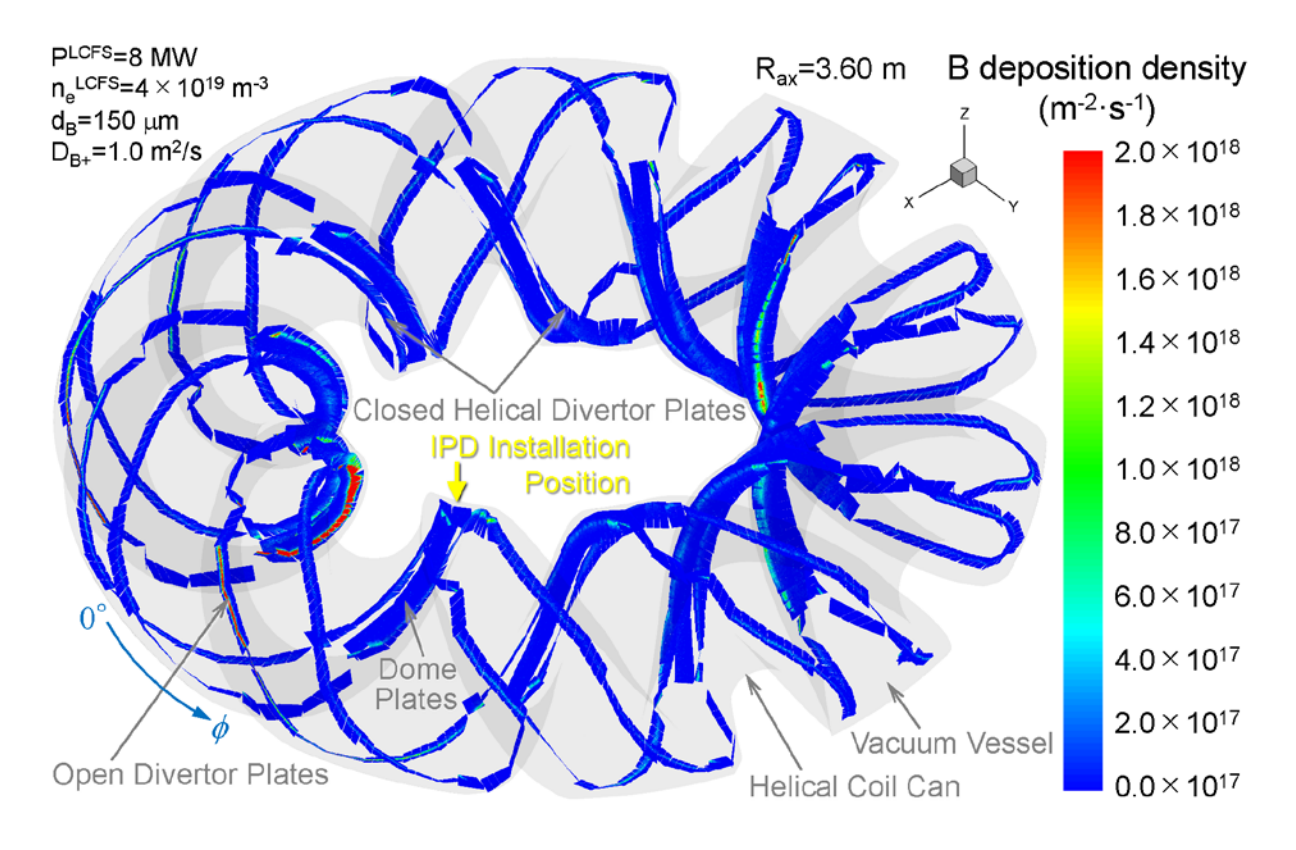


Fig. 3. A perspective view of the simulation result of the full-torus toroidal and poloidal distribution of the boron areal density deposited on the divertor components (the closed helical divetor plates, open divertor plates, and the dome plates) for the boron powder size  $d_{\rm B}$ =150 µm, the plasma density  $n_{\rm e}^{\rm LCFS}$ =4×10<sup>19</sup> m<sup>-3</sup>, and the plasma heating power  $P^{\rm LCFS}$ =8 MW. The shape of the vacuum vessel is displayed as semi-transparent surfaces. The boron deposition on the vacuum vessel and that on the back plates of the divertor components are not shown. It should be noted that the boron density deposited on the front surfaces of the divertor components can be seen from the backside in this figure. The IPD installation position on an upper port is approximately indicated as a yellow arrow.

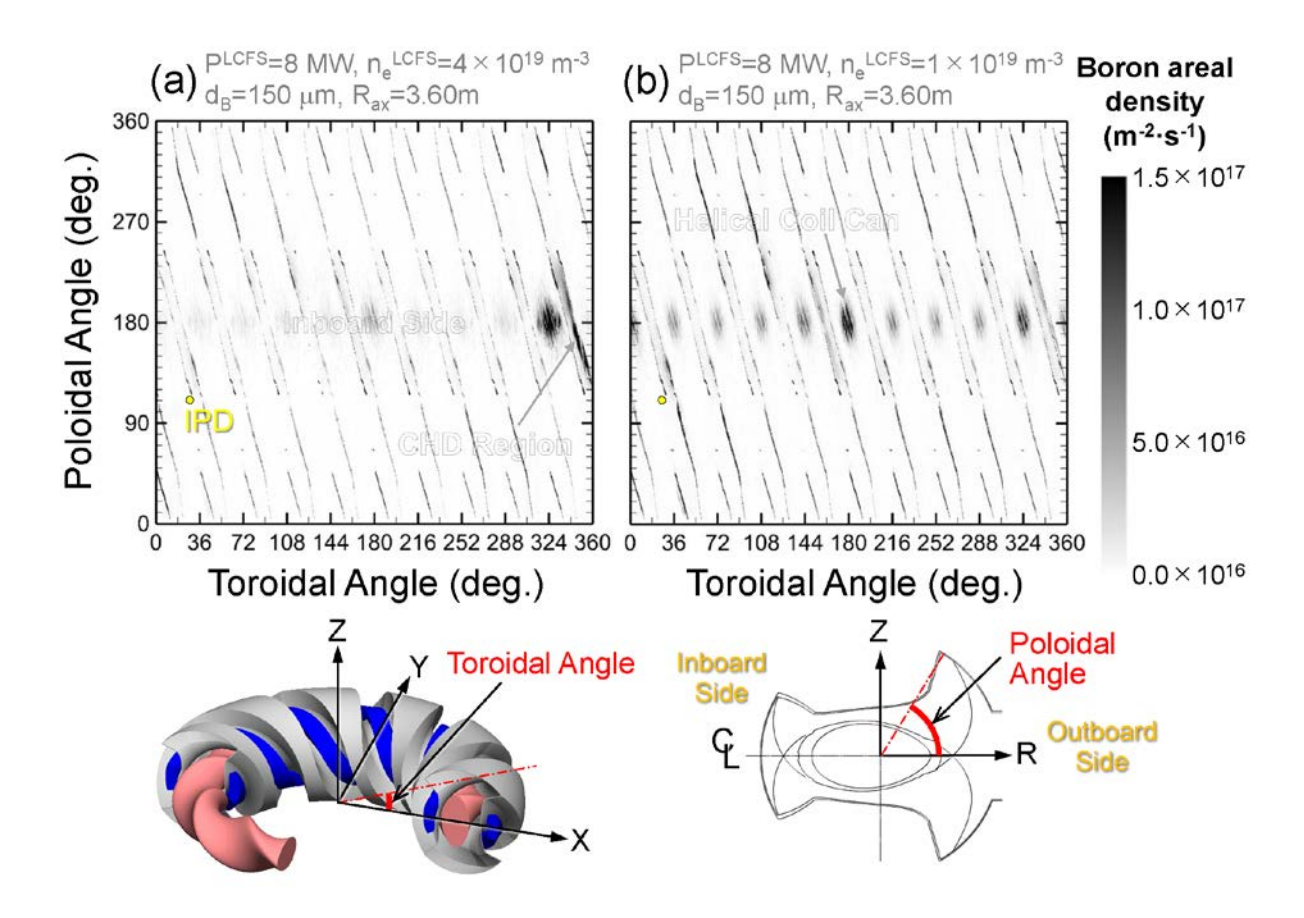


Fig. 4. The grey scale plot of the calculated boron areal density profile projected onto the full-tours toroidal and poloidal plane. The boron density deposited on the surface of the divertor components and the vacuum vessel is displayed for  $n_{\rm e}^{\rm LCFS}$ =1×10<sup>19</sup> m<sup>-3</sup> (a) and 4×10<sup>19</sup> m<sup>-3</sup> (b) under the condition of  $P^{\rm LCFS}$ =8 MW and  $d_{\rm B}$ =150 µm, respectively. The inboard side of the torus corresponds to the areas where the poloidal angle is around 180° in the toroidal and poloidal plane. The boron density deposited on the dome plates is not shown in this figure. The initial position for tracing the boron powder trajectories projected on the plane is approximately indicated as a small yellow circle.

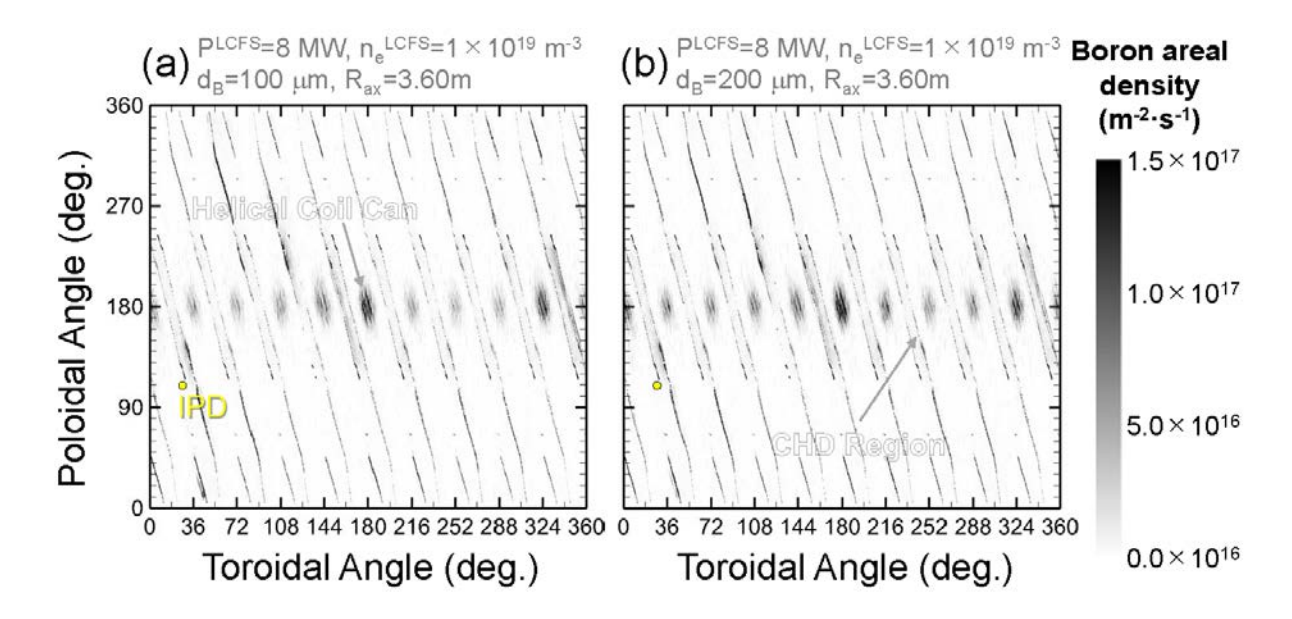
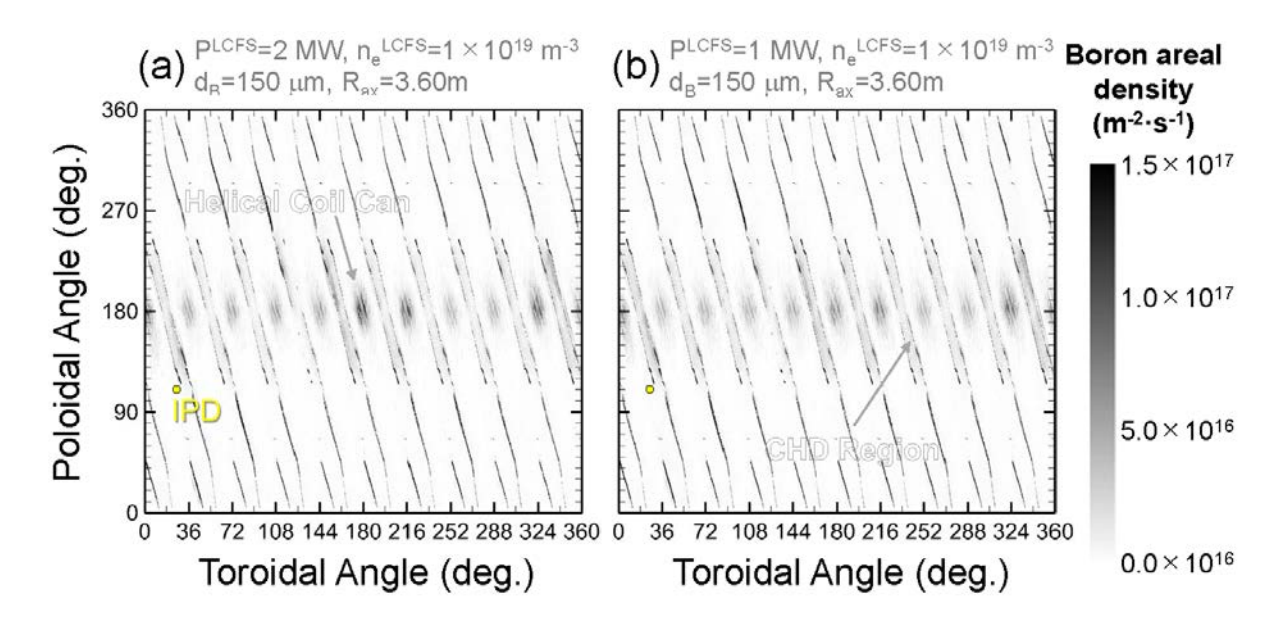


Fig. 5. The grey scale plot of the calculated boron areal density profile projected onto the full-tours toroidal and poloidal plane. The boron density deposited on the surface of the divertor components and the vacuum vessel is illustrated for the boron powder sizes  $d_{\rm B}$  of 100 μm (a) and 200 μm (b) under the condition of  $n_{\rm e}^{\rm LCFS}$ =1×10<sup>19</sup> m<sup>-3</sup> and  $P^{\rm LCFS}$ =8 MW, respectively.



**Fig. 6.** The grey scale plot of the calculated boron areal density profile projected onto the full-tours toroidal and poloidal plane. The boron density deposited on the surface of the divertor components and the vacuum vessel is shown for the two plasma heating powers  $P^{\rm LCFS}$  of 2 MW (a) and 1 MW (b) under the condition of  $n_{\rm e}^{\rm LCFS}$ =1×10<sup>19</sup> m<sup>-3</sup> and  $d_{\rm B}$ =150 µm, respectively.